Supporting Information for:

Ni/Co in and on CeO_2: A comparative study on dry reforming reaction

*Pradeep Kumar Yadav[a], Kalyani Patrikar[a], Dr. Anirban Mondal[a] and Dr. Sudhanshu Sharma[a]**

Department of Chemistry, Indian Institute of Technology Gandhinagar, Gandhinagar - 382355, India
**Corresponding authors:*
E-mail: ssharma@iitgn.ac.in

Number of Pages:31

Number of Figures: 15

Number of Tables: 06

Contents:

SI.7: Thermodynamic equilibrium conversion with Carbon formation calculations

SI.8: Long term H_2 and CO Yield curve for the dry reforming of methane over Ni supported over CeO_2, Co supported over CeO_2, Co-substituted CeO_2.

SI.9: Long term CH_4 and CO_2 conversion curve for the dry reforming of Co-substituted CeO_2

SI.10: TEM Analysis of spent catalysts

SI.11:TGA profiles of Ni/Co substituted and supported catalysts after CH_4 decomposition test

SI.12: Schematic sketch for mechanism on the basis of transient studies of methane decomposition and CO_2 reaction with deposited carbon after CH_4 decomposition on the Ni and Co supported the CeO_2.

SI.13: Schematic showing methane on Ni- and Co- substituted catalyst surface used to calculate adsorption energy at different sites

SI.14: Percentage CH_4 and CO_2 conversions for dry reforming of methane reaction at different flow rates for Co substituted CeO_2

SI.15*:* Apparent activation energy estimation for Co substituted CeO_2

Table S1. Rietveld refined structural parameters for CeO_2 substituted compounds

Table S2 -High-resolution Ce 3d XPS results. The listed-out figures are the binding energies (BE) and the area of each peak. The ratio of $Ce^{3+}/Ce^{4+}+Ce^{+3}$ was calculated to illustrate the content of oxygen vacancy around Ce^{3+} sites on the catalyst surface

Table S.3 O1s XPS peak deconvolution results of (a) Ni supported over CeO_2 (b) Co supported over CeO_2 (c) Ni substituted CeO_2 (d) Co substituted CeO_2

Table S.4 Summary of the Catalytic Activity in dry reforming of methane on the different Catalysts.

Table S.5 Selected Co based DRM catalysts reported in the literature and their activity

Table S.6 Amount of Carbon deposited by various catalyst in DRM with different Feed vol.% concentration (CH_4/CO_2=1)

1.Supporting Results:

SI.1:Zoomed XRD patterns for (a) Ni& Co substituted CeO_2 (b) Ni& Co supported CeO_2

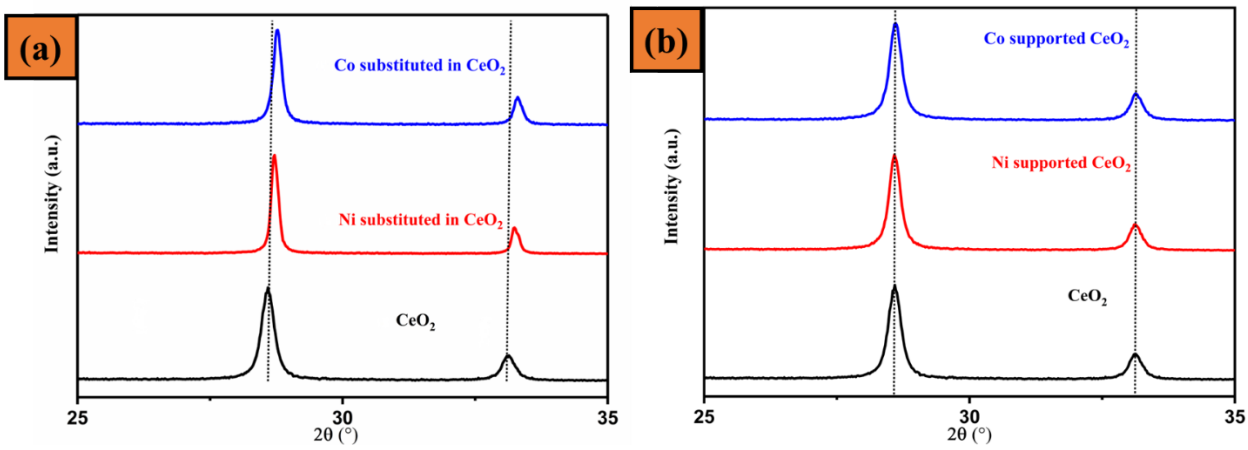

Figure S1 *– Zoomed XRD patterns for (a) Ni& Co substituted CeO_2 (b) Ni& Co supported CeO_2*

SI.2: Rietveld refined XRD patterns for (a) CeO_2 (b) Ni substituted CeO_2 (c) Co substituted CeO_2

Rietveld refinements (Figure S2) on the CeO_2 and transition metal (Ni, Co) substituted CeO_2 using the JANA 2006 software. The refinements were performed to approve the substitution of Ni and Co in CeO_2. Rietveld refinements have shown a considerable decrease in the lattice parameter and cell volume if we consider Ni and Co substitution on Ce site. The value of Goodness of fit (GOF) around unity specifies the admirable goodness of $Y_{observed}$ and $Y_{calculated}$ value[1] and authorizes that refined parameters are resolved even more absolutely. R(obs), R(all), and wR(all) are the reliability factor which also gave the information regarding the profile fitting.

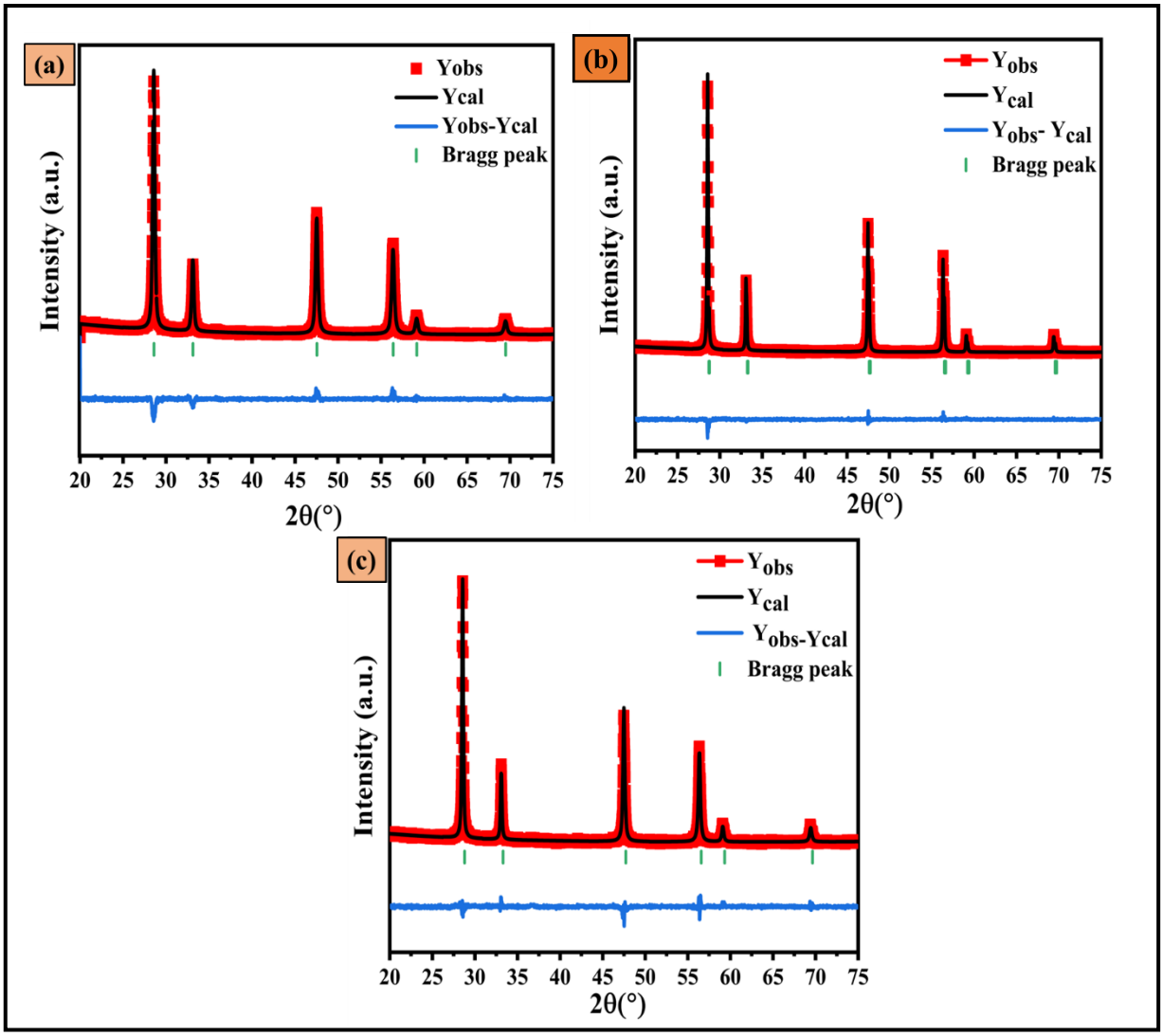
(a)
Yobs
Ycal
Yobs-Ycal
Bragg peak
Intensity (a.u.)
20 25 30 35 40 45 50 55 60 65 70 75
2θ(°)
(b)
Yobs
Ycal
Yobs- Ycal
Bragg peak
Intensity (a.u.)
20 25 30 35 40 45 50 55 60 65 70 75
2θ(°)
(c)
Yobs
Ycal
Yobs-Ycal
Bragg peak
Intensity (a.u.)
20 25 30 35 40 45 50 55 60 65 70 75
2θ(°)

substituted CeO_2

Table S1. *Rietveld refined structural parameters for CeO_2 substituted compounds*

Compounds	**CeO_2**	**Ni substituted CeO_2**	**Co substituted CeO_2**
Crystal System	FCC Cubic	FCC Cubic	FCC Cubic
Space group	Fm-3m (No: 225)	Fm-3m (No: 225)	Fm-3m (No: 225)
Lattice Parameters (Å)			
a=b=c	5.4182 (7)	5.4154 (3)	5.4103 (6)
Cell volume (Å³)	159.07 (3)	158.57 (13)	158.3 (3)
$R_{Factors}$			
R_{obs}	4.56	2.76	3.16
GOF	1.26	1.16	1.32
R_{all}	4.56	2.76	3.16
wR_{all}	4.72	3.38	3.76

SI.3: HR-TEM images of (a) Ni supported over CeO_2 (b) Co supported over CeO_2 (c) Ni substituted CeO_2 (d) Co substituted CeO_2. No indication of separated metal in substituted catalysts is apparent while the metallic Ni and Co are present in the supported catalysts

substituted CeO_2 (d) Co substituted CeO_2. No indication of separated metal in substituted catalysts is apparent while the metallic Ni and Co are present in the supported catalysts.

SI.4: High-angle annular dark-field (HAADF)-Scanning transmission electron microscopy and energy-dispersive X-ray elemental mapping of (a) Ni supported over CeO_2 (b) Co supported over CeO_2 (c) Ni substituted CeO_2 (d) Co substituted CeO_2

The morphology of deposited carbon on the spent catalyst after the reaction was carried out by the FEI Themis 60-300 with EDS detector and FEI CETA 4k x 4k camera for imaging the catalyst. Before performing the TEM analysis of catalysts were supported ultrasonically in methanol. A drop of dispersion was dropping cast over the carbon-coated copper grid and dried for two days.

Figure S4 shows Energy-dispersive X-ray spectroscopy (EDX) mapping of the (a) Ni supported over CeO_2 (b) Co supported over CeO_2 (c) Ni substituted CeO_2 (d) Co substituted CeO_2. The High-angle annular dark-field -Scanning transmission electron microscopy (HAADF-STEM) and corresponding EDX revealed a homogeneous elemental distribution and presence of Ni and Co supported over CeO_2 in figure S4 (a, b). The high-angle annular dark-field scanning transmission electron microscopy (HAADF-STEM) image (Figure S4c) of Ni substituted CeO_2 reveals that Ni aggregation is visible at some portion. The EDX of Ni distribution overall is low, but at some portion of concentration is high, possible reason for high concentration

intensity may be lot of particles stacked on each other. But from the XRD analysis we did not observe the separate phase of Ni or NiO. On the basis of that we are expecting most of Ni particle is substituted in the CeO_2. In the case Co substituted species are highly disseminated and no aggregation of Co is visible over CeO_2 structure as seen the Figure S4d.

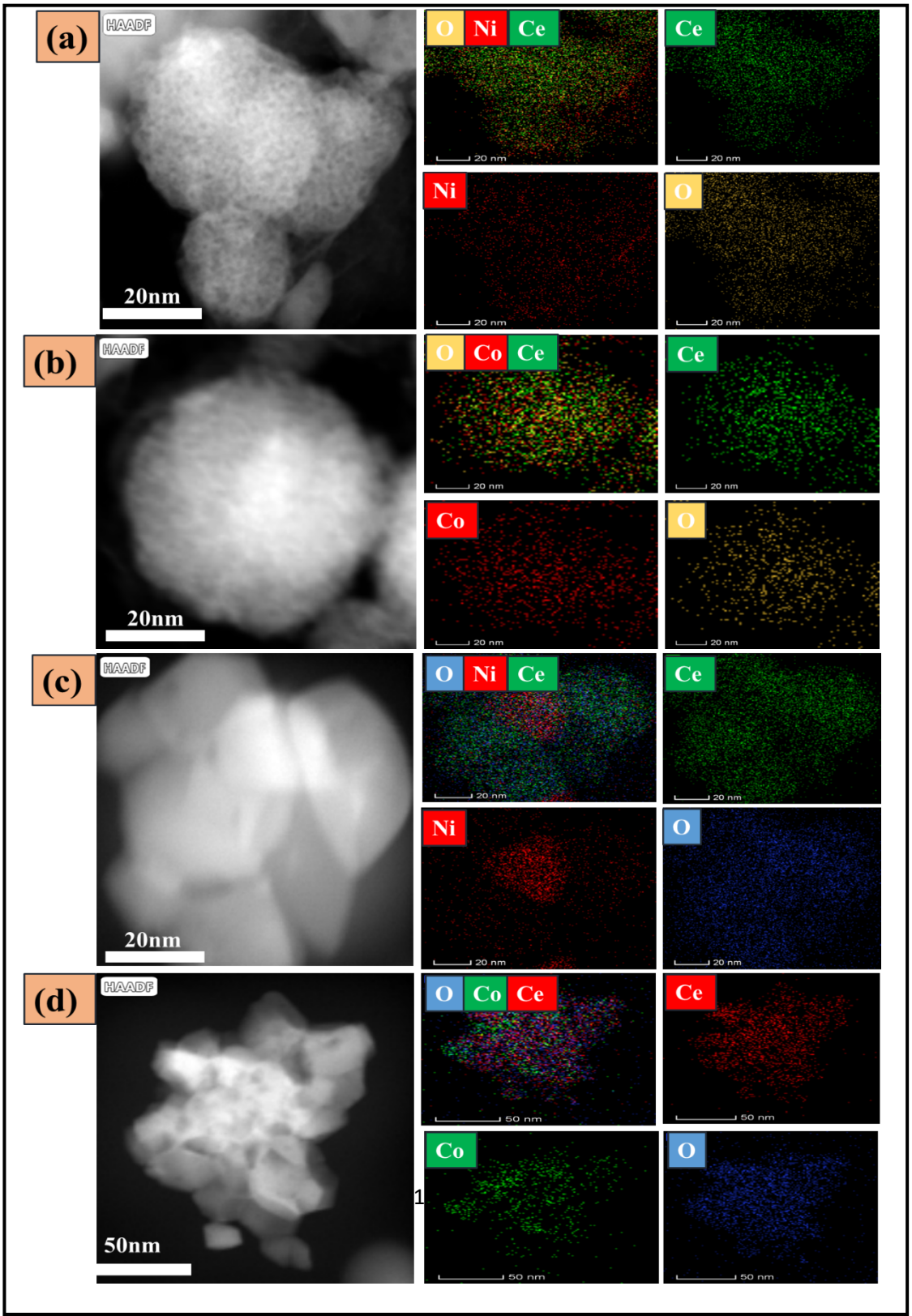

Figure S4: *High-angle annular dark-field-Scanning transmission electron microscopy (HAADF-STEM) and energy-dispersive X-ray elemental mapping of (a) Ni supported over CeO_2 (b) Co supported over CeO_2 (c) Ni substituted CeO_2 (d) Co substituted CeO_2*

SI.5: High resolution XPS spectra of Ce 3d in (a) Ni supported over CeO_2 (b) Co supported over CeO_2 (c) Ni substituted CeO_2 (d) Co substituted CeO_2

The complex XPS Ce 3d spectrum (FigureS5), explained in more detail somewhere else, was analysed following a procedure described in the literature. The Ce 3d spectrum was deconvoluted in 10 Gaussian-type functions with binding energies constrained to known values[2, 3]. Following notation introduced by Burroughs et al., The signals of Ce^{3+} are labelled as U′, U^0, V′, and V^0. In contrast, those of Ce^{4+} is labelled as U, U″, U‴, V, V″, and V‴, where the superscript corresponds to different final states, and the V and U correspond to the $3d_{5/2}$ and $3d_{3/2}$ states, respectively[4, 5]. The intensity of each peak permits the calculation of the Ce^{3+} fraction by using the equation-

$$\text{Ce (III)} = U^0 + U' + V^0 + V'$$

$$\text{Ce (IV)} = U + U'' + U''' + V + V'' + V'''$$

$$\text{Fraction of Ce (III) from Ce 3d} = \frac{Ce\ (III)}{Ce\ (IV)\ +\ Ce\ (III)}$$

The ratio between Ce^{3+} to Ce^{4+}+ Ce^{3+} concentration gives useful information regarding the presence of surface defects, that play a crucial role in determining the catalytic activity of Ceria based systems.

The fraction of Ce^{+3} is given in table(S2) for mono-metal substituted and supported catalyst. High-resolution Ce 3d XPS results and spectra are given in the Figure S5 and table S2 which listed-out the binding energies (BE) and the area of each peak. The ratio of Ce^{3+}/Ce^{4+}+Ce^{+3} was calculated to illustrate the content of oxygen vacancy around Ce^{3+} sites on the catalyst surface[6].

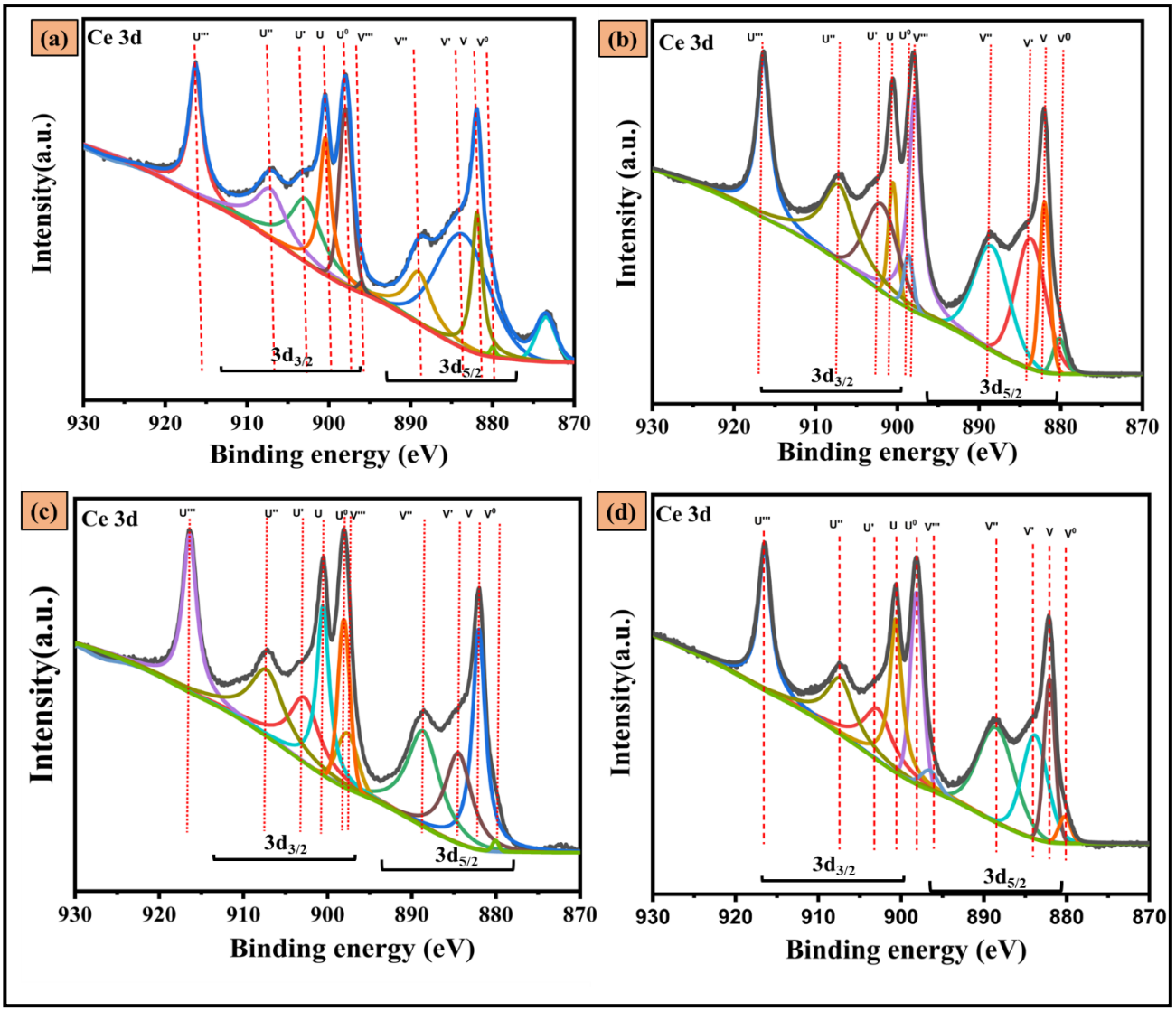
(a)
Ce 3d
U'''
U''
U'
U
U⁰
V''''
V''
V'
V
V⁰
3d3/2
3d5/2
Intensity(a.u.)
930
920
910
900
890
880
870
Binding energy (eV)
(b)
Ce 3d
U'''
U''
U'
U
U⁰
V''''
V''
V'
V
V0
3d3/2
3d5/2
Intensity (a.u.)
930
920
910
900
890
880
870
Binding energy (eV)
(c)
Ce 3d
U''''
U''
U'
U
U⁰
V''''
V''
V'
V
V⁰
3d3/2
3d5/2
Intensity(a.u.)
930
920
910
900
890
880
870
Binding energy (eV)
(d)
Ce 3d
U'''
U''
U'
U
U⁰
V''''
V''
V'
V
V⁰
3d3/2
3d5/2
Intensity(a.u.)
930
920
910
900
890
880
870
Binding energy (eV)

supported over CeO_2 (c) Ni substituted CeO_2 (d) Co substituted CeO_2

Table S2 -*High-resolution Ce 3d XPS results. The listed-out figures are the binding energies (BE) and the area of each peak. The ratio of $Ce^{3+}/Ce^{4+}+Ce^{+3}$ was calculated to illustrate the content of oxygen vacancy around Ce^{3+} sites on the catalyst surface*

Peaks assignment	Binding energy (eV)	Ni supported over CeO_2	Co supported over CeO_2	Ni-substituted CeO_2	Co-substituted CeO_2
V^0	**880.7-881.2**	2145.2	3060.9	3671.3	3602.6
V	**882.7-883.9**	52795.6	221848.1	213387.8	65087.2
V'	**885.3-886.9**	115195.6	78986.4	141609.8	146203.7
V''	**888.6-889.9**	155738.1	71240.3	184317.3	173939.7
V'''	**898.1-899**	105698.3	4047.0	58504.6	3502.6
U^0	**899.1-899.9**	71260.5	88156.4	101659.0	200628.8
U	**900.8-900.9**	81176.9	87344.2	156351.3	122856.7
U'	**903.7-903.9**	45166.5	108933.0	143628.8	80969.2
U''	**907.3-908**	156190.6	86343.2	173856.6	151613.5
U'''	**916.7-917.3**	127736.0	91573.4	166848.1	160017.6
	Ce^{+3}	233767.8	279136.7	390568.9	431404.3
	Ce^{+4}	679335.5	562396.2	953265.7	677017.3
	Fraction Ce (III) from Ce 3d = $\frac{Ce\ (III)}{Ce\ (IV)\ +\ Ce}$	0.25	0.33	0.29	0.38

SI.6: High resolution XPS spectra of O 1s in (a) Ni supported over CeO_2 (b) Co supported over CeO_2 (c) Ni substituted CeO_2 (d) Co substituted CeO_2

The O 1s XPS show two different types of oxygen species for supported catalysts, but substituted catalysts show three different types of oxygen species. The detected main peak labelled as O′ at 529.01-529.5eV was the lattice oxygen in metal oxide, and a shoulder labelled as O″ at 531.01-531.9.5eV was ascribed to the chemically adsorbed oxygen[3, 7]. The peak at 532.01-532.9eV (O’’’) can be ascribed water/carbonate species multiplicity of physiosorbed and chemisorbed water on or near the surface, respectively[8]. Upon incorporation of Ni or Co in the CeO_2, increase the instability of O species (lattice oxygen – O') occurs which generates the active oxygen species ($O_{\cdot}$, O^{2-}, and O^{-}) in CeO_2. As oxygen vacancy density could facilitate oxygen species adsorption(O")[9].So another word if more will be oxygen vacancies, more will be chemically adsorbed oxygen. The ratios of O″/O′ for supported and substituted samples suggested that more active Oxygen vacancy on the ceria surface[10]. Occurrence of Ce^{3+} being related to oxygen vacancy formation, the higher Ce^{3+} concentration in the catalyst should indicate more generation of oxygen vacancies. High-resolution O1s XPS results and spectra are given in the Figure S8 and table S3 which listed-out the binding energies (BE) and the area of each peak. The ratio of O’’/O’ or absorbed oxygen to the lattice oxygen was calculated to illustrate the content of oxygen vacancy around Ce^{3+} sites on the catalyst surface. The surface chemical state of Ce 3d and the high percentage of Ce^{3+} imply the existence of non-stoichiometric oxygen vacancy[3, 8].

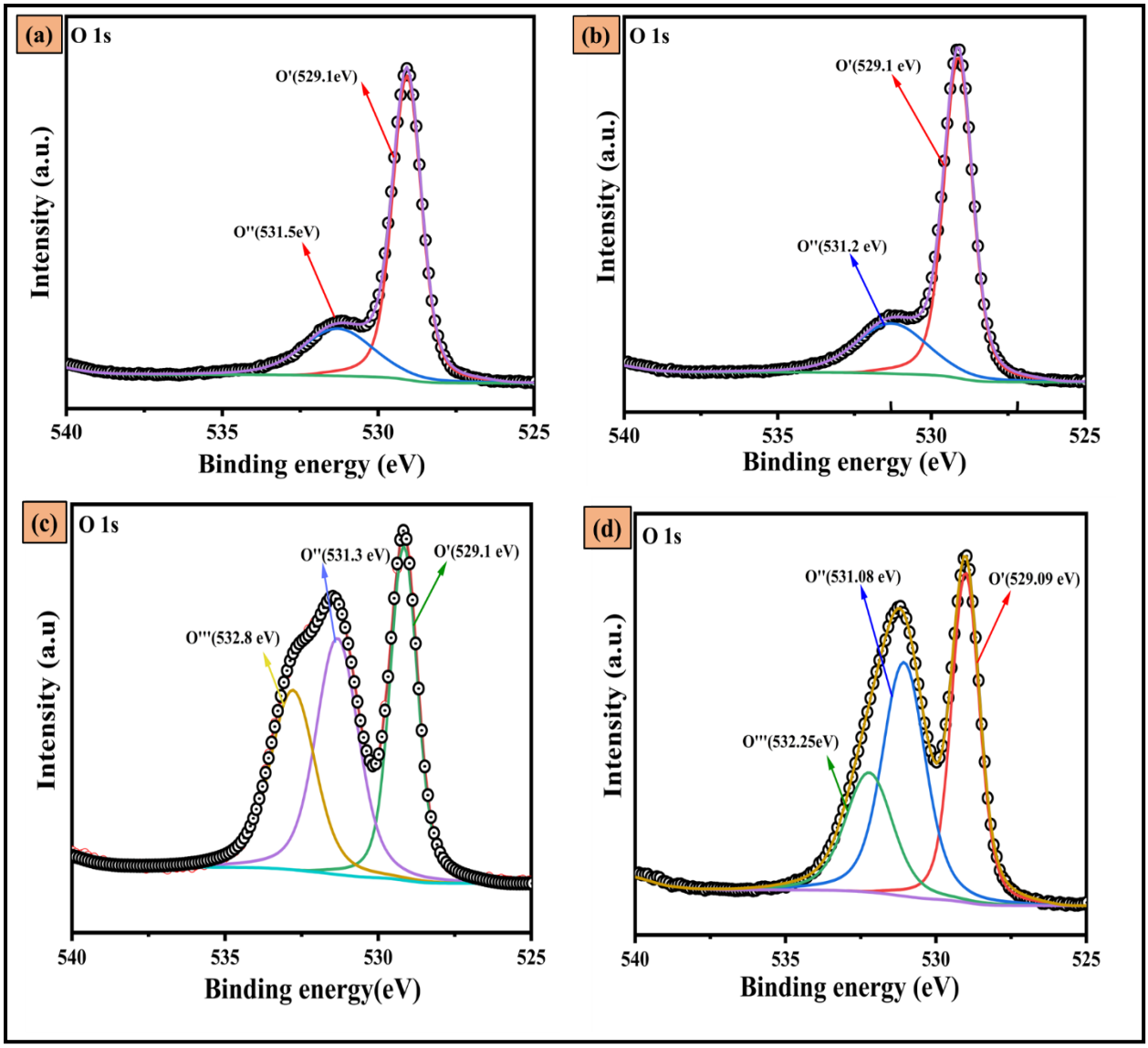
(a)
O 1s
O'(529.1eV)
O''(531.5eV)
Intensity (a.u.)
540
535
530
525
Binding energy (eV)
(b)
O 1s
O'(529.1 eV)
O''(531.2 eV)
Intensity (a.u.)
540
535
530
525
Binding energy (eV)
(c)
O 1s
O''(531.3 eV)
O'(529.1 eV)
O'''(532.8 eV)
Intensity (a.u)
540
535
530
525
Binding energy(eV)
(d)
O 1s
O''(531.08 eV)
O'(529.09 eV)
O'''(532.25eV)
Intensity (a.u.)
540
535
530
525
Binding energy (eV)

***Figure S6**: shows the O 1s XPS spectra of (a) Ni supported over CeO_2 (b) Co supported over CeO_2 (c) Ni substituted CeO_2 (d) Co substituted CeO_2*

***Table S.3** O1s XPS peak deconvolution results of (a) Ni supported over CeO_2 (b) Co supported over CeO_2 (c) Ni substituted CeO_2 (d) Co substituted CeO_2*

Peaks assignment	**Binding energy (eV)**	**Ni supported over CeO_2 (Area)**	**Co supported over CeO_2 (Area)**	**Ni-substituted CeO_2 (Area)**	**Co-substituted CeO_2 (Area)**
O’	529.01-529.5eV	140037.13	178677.3	86936.96	105438.32
O’’	531.01-531.9.5eV	53095.17	69274.17	95464.25	144595.24
O’’’	532.01-532.9eV	-	-	76314	64631.9
O’’/O’		0.37915066	0.38771	1.09809	1.371373

Table

Catalyst	Maximum conversion of CH_4 at 800 ^oC (%)	Maximum conversion of CO_2 at 800 ^oC (%)	H_2/CO at 800 ^oC	Loss in conversion and Yield after 300 minutes (%)			
				CH_4	CO_2	CO	H_2
Ni Supported CeO_2	100	84	0.5	15	12	18	11
Co Supported CeO_2	98	91	0.6	4	5	9	11
Ni Substituted CeO_2	-	-	-	-	-	-	-
Co Substituted CeO_2	90.2	97	0.8	6	5	7	6

S.4 *Summary of the Catalytic Activity in dry reforming of methane on the different Catalysts*

Catalysts	Preparation Method	Reaction condition	Conversion		Reference
			CH_4	CO_2	
Co substituted CeO_2	Solution combustion method	Temperature=800^0C, 1atm, $CH_4/CO_2/N_2$ =1/1/18 and the flow rate was 20mLmin^{-1}, GHSV =~12000 h^{-1} TOS=20hours	90%	92%	This work
Co/CeO_2	Incipient wetness impregnation method	700 °C with 50 sccm CH_4: CO2: Ar (1:1:3) gas flow TOS=5 h.	20%	25%	[11]

Table S.5 *Selected Co based DRM catalysts reported in the literature and their activity*

Co/TiO_2	Incipient wetness impregnation method	CH_4/CO_2=1; 1023 K; 2.0 MPa;	~28%	-	[12]
$26Co/ZrO_2$	Incipient wetness impregnation method	CH4/CO2/He (10:10:80 in volume). T=750 °C	85%	-	[13]
$Co/\gamma\text{-}Al_2O_3$	Incipient wetness impregnation method	(CH4/CO2 =1/1) flow rate =20 ml/min T=900 °C	90%	-	[14]
$15Co/Al_2O_3$	Incipient wetness impregnation method	CH_4: CO2: N_2 = 1:1:3 (vol ratio), temperature = 873 K.	20%	-	[15]
Co/SiO_2	Incipient wetness impregnation method oleyl amine/oleic acid	T=700 °C $CH_4/CO_2/N_2$=33.3:33.3:33.3	30%	30%	[16]
Co/SiO_2 derived from	Hydrothermal	T = 750 °C, He: CH4: CO2 = 1:1:1 with a total	5%	10%	[17]

phyllosilicates	method	flow rate of 30 ml/min			
Co/MgO-Al_2O_3 from hydrotalcite	Incipient wetness impregnation method	T=800 °C CH_4/CO_2=40:60	20%	20%	[18]
Co/ZSM-5	Incipient wetness impregnation method	T=800 °C CH_4/CO_2/=20:20:60	65%	75%	[19]

SI.7: Thermodynamic equilibrium conversion with Carbon formation calculations:

Total Gibbs free energy minimization was employed to evaluate the thermodynamics of dry reforming reaction using Aspen Plus V9, Aspen Tech.

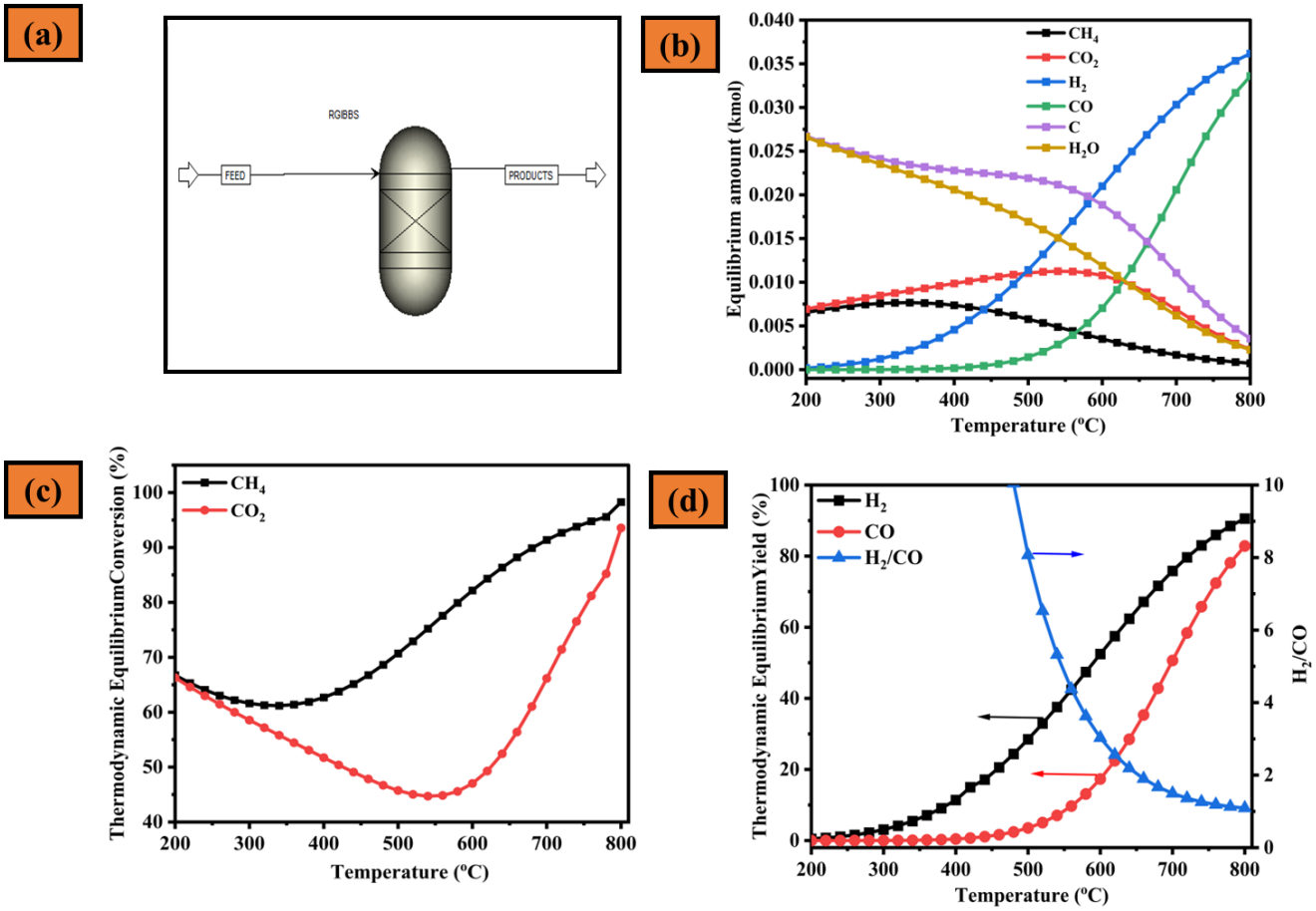

Figure.S7. *(a)Flowsheet used in Aspen Plus simulation to carry out thermodynamic calculations via the Gibbs free energy minimization method. (b) Equilibrium composite (c) Equilibrium conversion of CH_4 And CO_2 (d) Equilibrium Yield of H_2 And CO. All results were obtained by considering carbon formation. Feedstock: 0.020 kmol CH_4 +0.020 kmol CO_2 as per our results obtained from GC Pressure:1 atm; Temperature: 200-800 ^{O}C.*

SI.8: Long term H_2 and CO Yield curve for the dry reforming of methane over Ni supported over CeO_2, Co supported over CeO_2, Co-substituted CeO_2

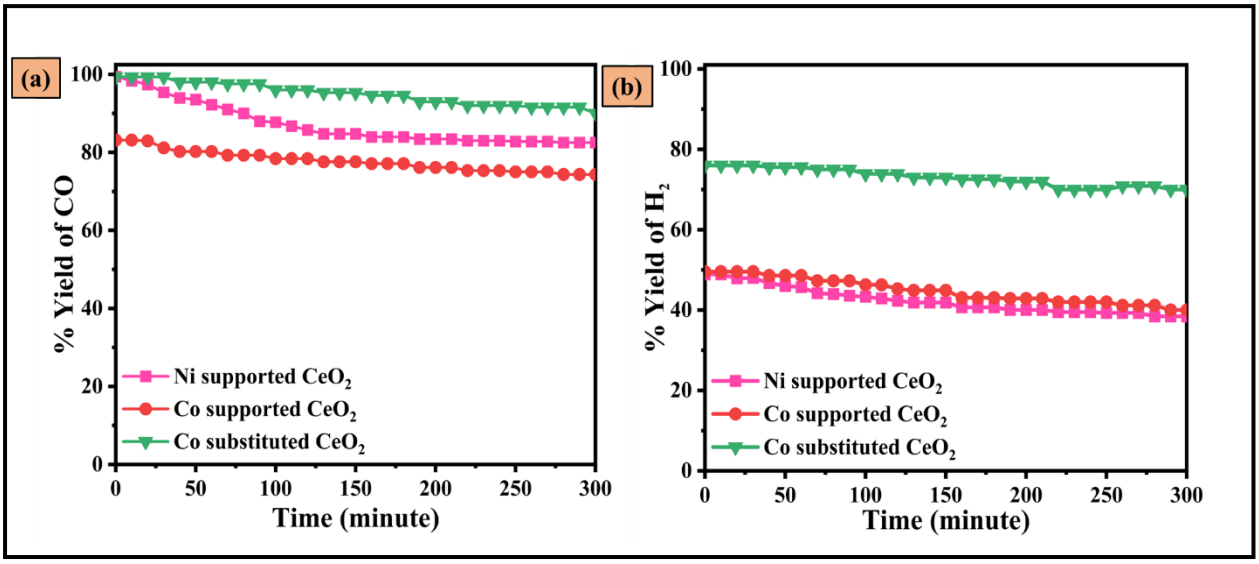

Figure S8: *Catalytic activity for the dry reforming of methane: (a) CO Yield (b) H_2 Yield as function of temperature. Reaction condition: Temperature=800^{0}C, 1atm, $CH_4/CO_2/N_2$ =1/1/18 and the flow rate was 20mLmin^{-1}, GHSV =~12000mL/(g.h) For Ni supported over CeO_2, Co supported over CeO_2, Co-substituted CeO_2.*

SI.9: Long term CH_4 and CO_2 conversion curve for the dry reforming of Co-substituted CeO_2

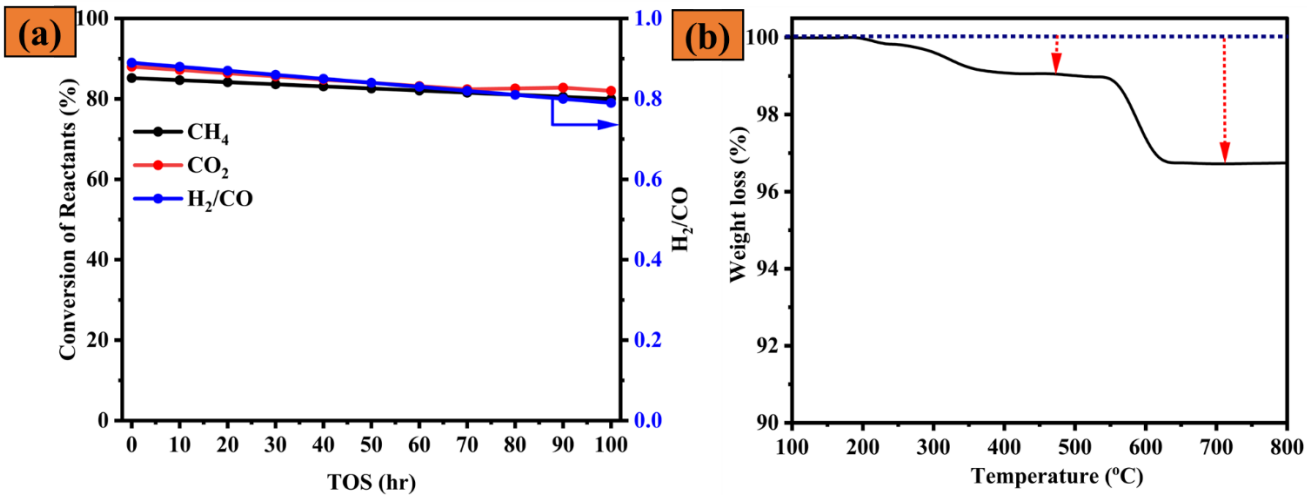

Catalyst	CH_4/CO_2 (Vol.%)	GHSV	Operating Temperature (T^oC)	TOS (hr.)	Amount of Deposited Carbon After the reaction (by TGA)	Ref.
Co substituted CeO_2	30/30	*12000mL/(g.h)*	750	100	3.7 %	**This work**
5 wt. % Ni/14.7 wt. % Ce - SBA-16	33/33	30,000 mL h^{-1} g_{cat}^{-1}	700	50	7%	[20]
12 wt.% $Ni/Ce_{0.8}Gd_{0.2}O_2$	33/33	28,800 h^{-1}	800	100	18%	[21]
Ni/CeO_2	40/40	150,000 mL h^{-1} g_{cat}^{-1}	800	50	19.4%	[22]
Ni/Zr-DC	40/40	150,000 mL	800	50	13.6%	[22]

Figure S9: *Catalytic activity for the dry reforming of methane: CO_2 and CH_4 conversion as function of temperature. Reaction condition: Temperature=750 ^oC, 1atm, $CH_4/CO_2/N_2$ =6/6/8 and the flow rate were 20mLmin^{-1}, GHSV =~12000mL/ (g.h) (b) TGA curve after the 100hr TOS for Co-substituted CeO_2*

Table S6. Amount of Carbon deposited by various catalyst in DRM with different Feed vol.% concentration (CH_4/CO_2=1)

		$h^{-1}\ g_{cat}^{-1}$				
Ni/Sm-DC	40/40	150,000 mL $h^{-1}\ g_{cat}^{-1}$	800	50	3.3%	22
Ni/La-DC	40/40	150,000 mL $h^{-1}\ g_{cat}^{-1}$	800	50	2.0%	22
Ni/*mp*-$Ce_{1-x}Ni_xO_{2-y}$	50/50	12 000 mL (h g_{cat}) $^{-1}$	700	40	10%	23
Ni/*n*-$Ce_{1-x}Ni_xO_{2-y}$	50/50	12 000 mL (h g_{cat}) $^{-1}$	700	40	20%	23
Ni–Al	50/50	36,000 mL $h^{-1}\ g^{-1}_{cat}$	700	80	15%	24
Ni–1Ce–Al	50/50	36,000 mL $h^{-1}\ g^{-1}_{cat}$	700	80	16%	24
Ni–2Ce–Al	50/50	36,000 mL $h^{-1}\ g^{-1}_{cat}$	700	80	12%	24
Ni/Al-IMP	50/50	36,000 mL $h^{-1}\ g^{-1}_{cat}$	700	80	52%	24
Ni/Ce–Al-IMP	50/50	36,000 mL	700	80	22.5%	24
Co/C						11
NiCo/C						11
CoNi/T			-1			12

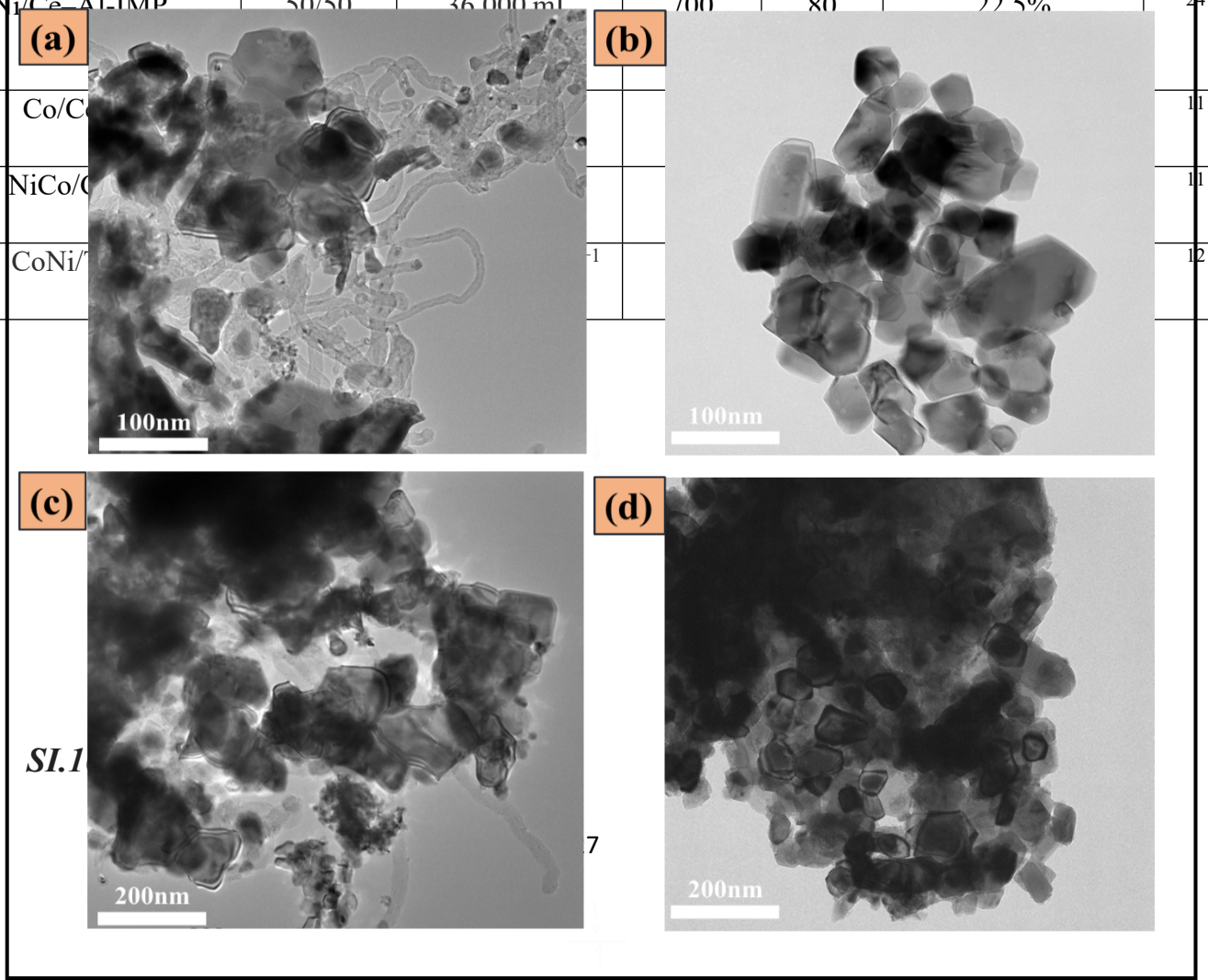

SI.1

***Figure S 10**: TEM images of spent catalyst- (a) Ni supported over CeO_2 (b) Co supported over CeO_2 (c) Ni substituted CeO_2 (d) Co substituted CeO_2 Reaction condition: Temperature=800^0C, 1atm, $CH_4/CO_2/N_2$ =1/1/18 and the flow rate was 20mLmin^{-1}, GHSV =12000mL/(g.h)*

SI.11:TGA profiles of Ni/Co substituted and supported catalysts after CH_4 decomposition test

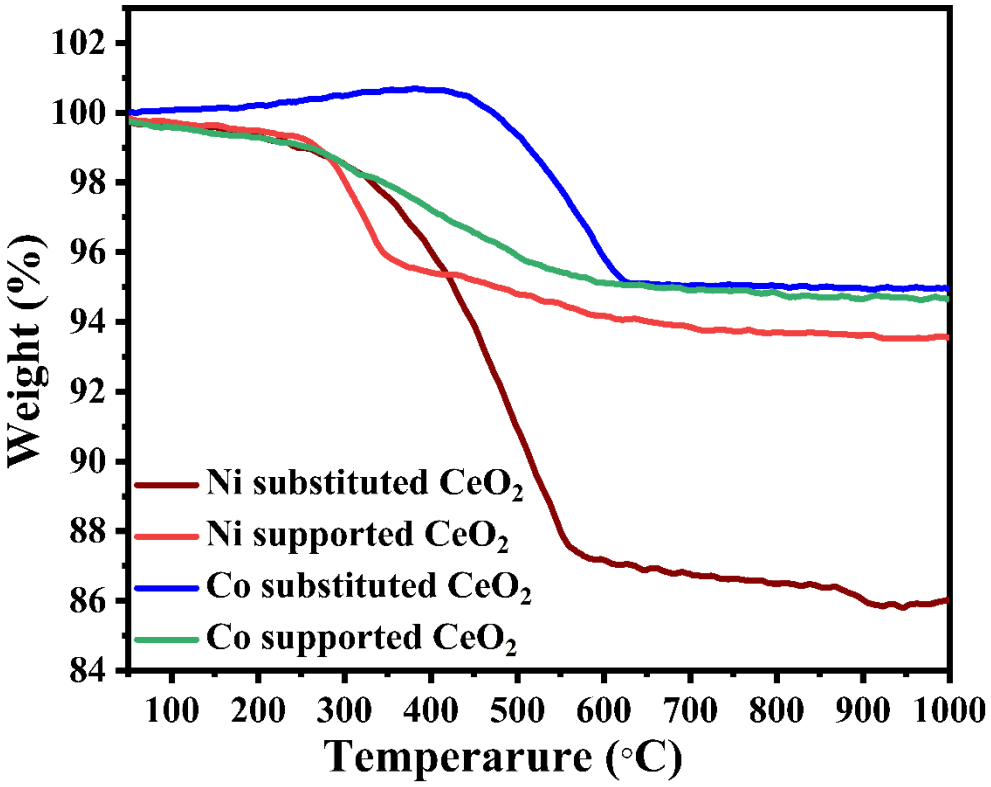

***Figure S11:**TGA profiles of Ni/Co substituted and supported catalysts after CH_4 decomposition test*

SI.12: Schematic sketch for mechanism on the basis of transient studies of methane decomposition and CO_2 reaction with deposited carbon after CH_4 decomposition on the Ni and Co supported the CeO_2.

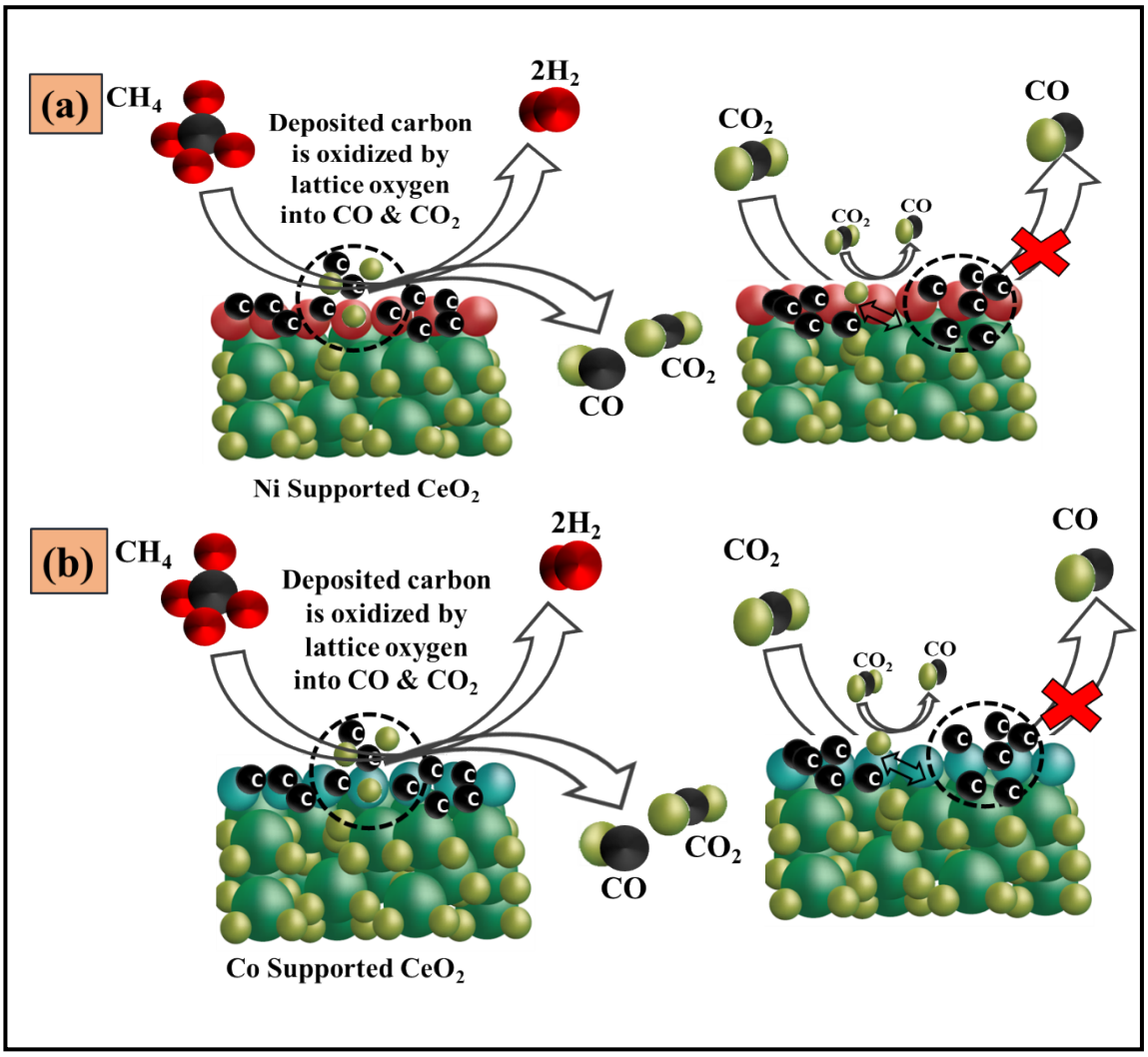

Figure S12: *Schematic sketch for mechanism on the basis of transient studies of methane decomposition and CO_2 reaction with deposited carbon after CH_4 decomposition on the Ni and Co supported the CeO_2.*

SI.13: Schematic showing methane on Ni- and Co- substituted catalyst surface used to calculate adsorption energy at different sites

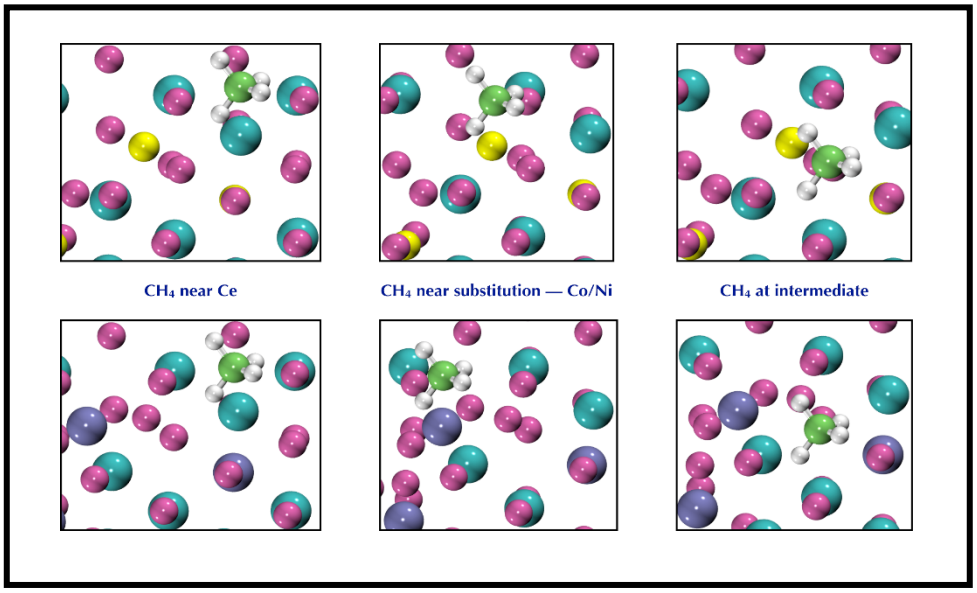

Figure S13*: Schematic showing methane on Ni- and Co-substituted catalyst surface used to calculate adsorption*

energy at different sites.

SI.14: Percentage CH_4 and CO_2 conversions for dry reforming of methane reaction at different flow rates for Co substituted CeO_2

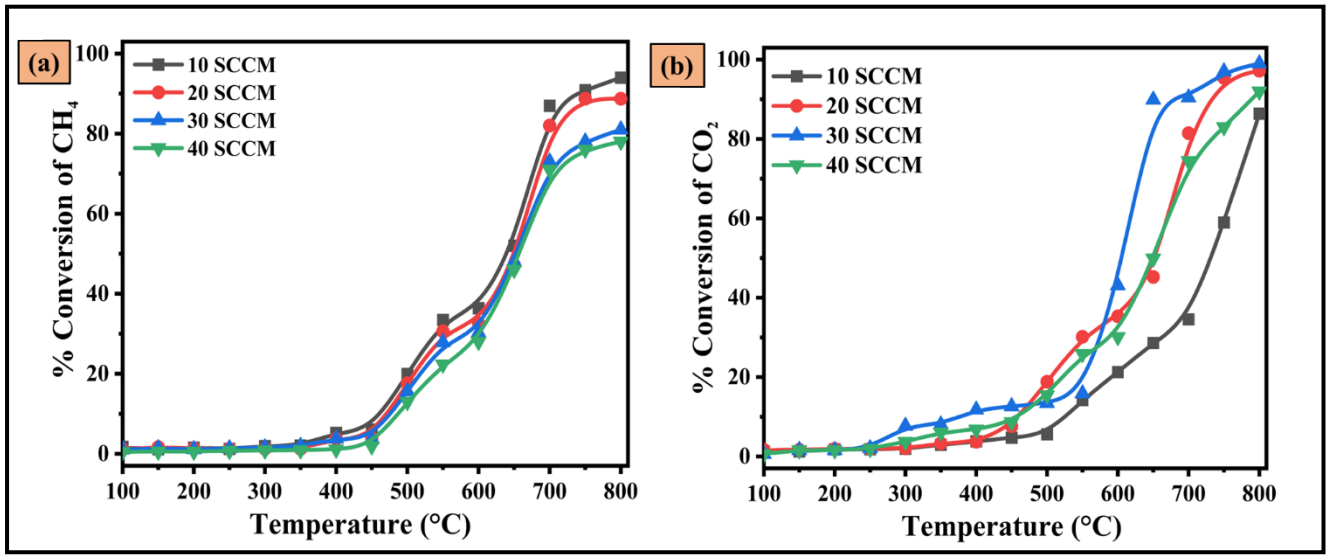

Figure S14: *Percentage CH_4 and CO_2 conversions for dry reforming of methane reaction at different flow rates for Co substituted CeO_2*

SI.15: Apparent activation energy estimation for Co substituted CeO_2

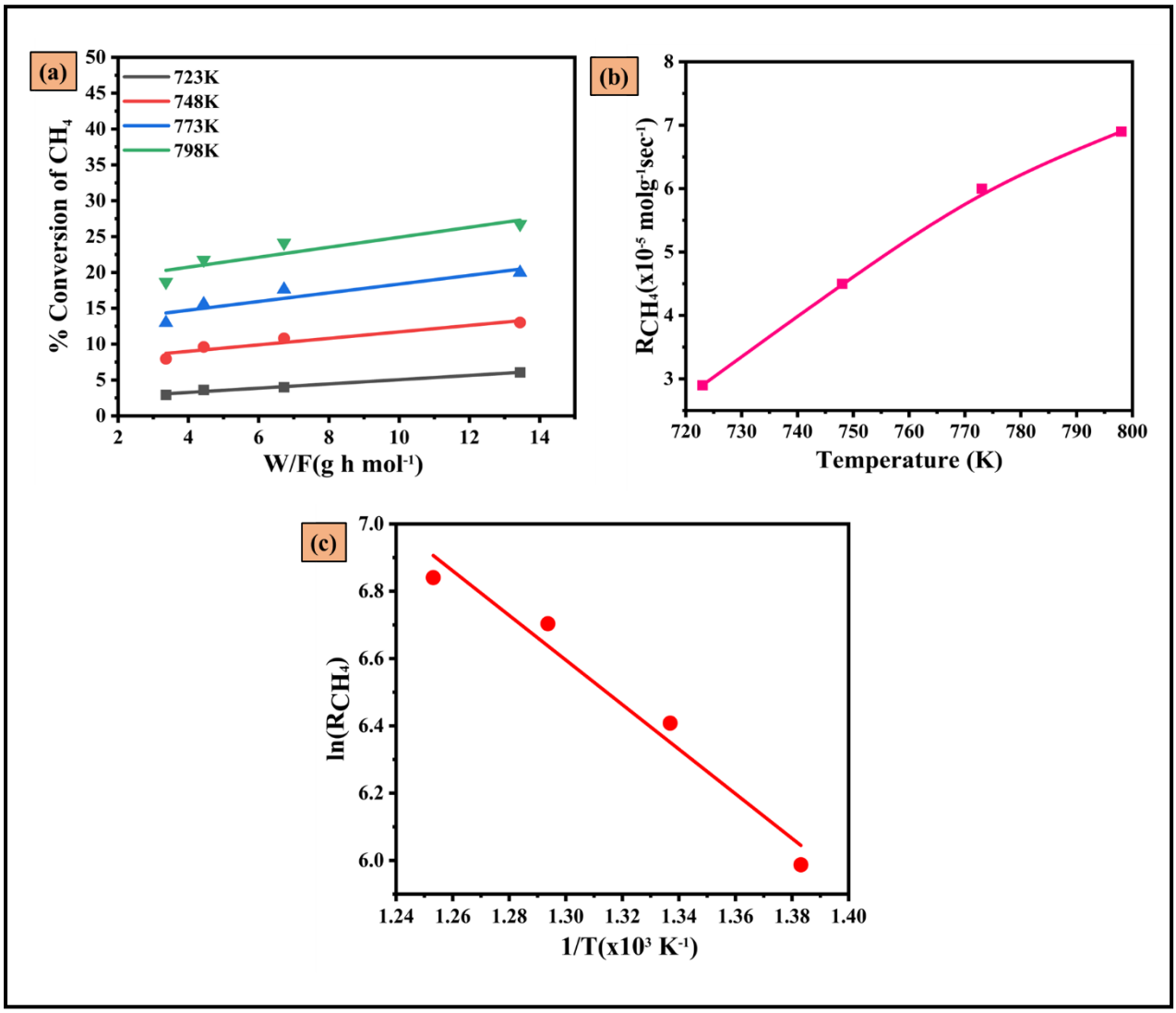

Figure S15: *(a) Effects of space-time (W/F) on % conversion of methane at different temperature (b)Reaction rate curve (c)Arrhenius plots of dry reforming of methane over Co Substituted CeO_2 catalyst. Reaction conditions: T = 723–798 K, $CH_4/CO_2/N_2$=1/1/18, Catalyst 100 mg*

2- Reference:

1. M. Sukumar, L. J. Kennedy, J. J. Vijaya, B. Al-Najar and M. Bououdina, *New Journal of Chemistry*, 2018, **42**, 18128-18142.
2. N. K. Eswar, V. V. Katkar, P. C. Ramamurthy and G. Madras, *Industrial & Engineering Chemistry Research*, 2015, **54**, 8031-8042.
3. S. Sultana, S. Mansingh, M. Scurrell and K. M. Parida, *Inorganic Chemistry*, 2017, **56**, 12297-12307.
4. A. Q. Wang, P. Punchaipetch, R. M. Wallace and T. D. Golden, *Journal of Vacuum Science & Technology B: Microelectronics and Nanometer Structures Processing, Measurement, and Phenomena*, 2003, **21**, 1169-1175.
5. P. Burroughs, A. Hamnett, A. F. Orchard and G. Thornton, *Journal of the Chemical Society, Dalton Transactions*, 1976, DOI: 10.1039/DT9760001686, 1686-1698.
6. Z. Wu, M. Li, J. Howe, H. M. Meyer and S. H. Overbury, *Langmuir*, 2010, **26**, 16595-16606.
7. A. Velamakanni, K. J. Ganesh, Y. Zhu, P. J. Ferreira and R. S. Ruoff, *Advanced Functional Materials*, 2009, **19**, 3926-3933.
8. S. Mansingh, D. K. Padhi and K. M. Parida, *Catalysis Science & Technology*, 2017, **7**, 2772-2781.
9. F. Zhao, S. Li, X. Wu, R. Yue, W. Li and Y. Chen, *RSC Advances*, 2019, **9**, 2343-2352.
10. S. A. Ansari, M. M. Khan, M. O. Ansari, S. Kalathil, J. Lee and M. H. Cho, *RSC Advances*, 2014, **4**, 16782-16791.

11. H. Ay and D. Üner, *Applied Catalysis B: Environmental*, 2015, **179**, 128-138.
12. K. Nagaoka, K. Takanabe and K.-i. Aika, *Applied Catalysis A: General*, 2004, **268**, 151-158.
13. V. M. Gonzalez-delaCruz, R. Pereñiguez, F. Ternero, J. P. Holgado and A. Caballero, *The Journal of Physical Chemistry C*, 2012, **116**, 2919-2926.
14. E. Ruckenstein and H. Y. Wang, *Journal of Catalysis*, 2002, **205**, 289-293.
15. S. Sengupta, K. Ray and G. Deo, *International Journal of Hydrogen Energy*, 2014, **39**, 11462-11472.
16. X. Gao, Z. Tan, K. Hidajat and S. Kawi, *Catalysis Today*, 2017, **281**, 250-258.
17. Z. Bian and S. Kawi, *Journal of CO2 Utilization*, 2017, **18**, 345-352.
18. J. Xu, W. Zhou, Z. Li, J. Wang and J. Ma, *International Journal of Hydrogen Energy*, 2009, **34**, 6646-6654.
19. J. Estephane, S. Aouad, S. Hany, B. El Khoury, C. Gennequin, H. El Zakhem, J. El Nakat, A. Aboukaïs and E. Abi Aad, *International Journal of Hydrogen Energy*, 2015, **40**, 9201-9208.
20. S. Zhang, S. Muratsugu, N. Ishiguro and M. Tada, *ACS Catalysis*, 2013, **3**, 1855-1864.
21. H. R. Gurav, S. Dama, V. Samuel and S. Chilukuri, *Journal of CO2 Utilization*, 2017, **20**, 357-367.
22. I. Luisetto, S. Tuti, C. Romano, M. Boaro, E. Di Bartolomeo, J. K. Kesavan, S. S. Kumar and K. Selvakumar, *Journal of CO2 Utilization*, 2019, **30**, 63-78.
23. J. Deng, W. Chu, B. Wang, W. Yang and X. S. Zhao, *Catalysis Science & Technology*, 2016, **6**, 851-862.
24. N. Wang, K. Shen, L. Huang, X. Yu, W. Qian and W. Chu, *ACS Catalysis*, 2013, **3**, 1638-1651.